

Distinguishing genelet circuit input pulses via a pulse detector

Colin Yancey¹ · Rebecca Schulman^{1,2,3}

Accepted: 9 May 2024 © The Author(s) 2024

Abstract

Chemical systems have the potential to direct the next generation of dynamic materials if they can be integrated with a material while acting as the material's own regulatory network. Chemical networks that use DNA and RNA strand displacement coupled with RNA synthesis and degradation, such as genelets, are promising chemical systems for this role. Genelets can produce a range of dynamic behaviors that respond to unique sets of environmental inputs. While a number of networks that generate specific types of outputs which vary in both time and amplitude have been developed, there are fewer examples of networks that recognize specific types of inputs in time and amplitude. Advanced chemical circuits in biology are capable of reading a given substrate concentration with relatively high accuracy to direct downstream function, demonstrating that such a chemical circuit is possible. Taking inspiration from this, we designed a genelet circuit which responds to a range of inputs by delivering a binary output based on the input concentration, and tested the network's performance using an in silico model of circuit behavior. By modifying the concentrations of two circuit elements, we demonstrated that such a network topography could yield various target input concentration profiles to which a given circuit is sensitive. The number of unique elements in the final network topography as well as the individual circuit element concentrations are commensurate with properties of circuits that have been demonstrated experimentally. These factors suggest that such a network could be built and characterized in the laboratory.

Keywords DNA nanotechnology · Molecular computing · DNA circuits · Genelets

Mathematics Subject Classification 94C60

1 Introduction

Genetic regulatory networks (GRNs) are ubiquitous in biology because of their ability to interact with dynamic environments in which biological systems reside. GRNs regulate everything from resource management in cells in response to nutrient deficiencies (Ueda et al. 2020) to the differentiation of totipotent cell lines during embryogenesis

Rebecca Schulman rschulm3@jhu.edu Colin Yancey

Colin Yancey cyancey7@jhu.edu

Published online: 20 June 2024

- Department of Chemical and Biomolecular Engineering, Johns Hopkins University, Baltimore, MD, USA
- Department of Computer Science, Johns Hopkins University, Baltimore, MD, USA
- Department of Chemistry, Johns Hopkins University, Baltimore, MD, USA

(Sladitschek and Neveu 2019; Gregor et al. 2007a). Embryogenesis circuits have been shown to be quite sophisticated, capable of effectively measuring the absolute concentrations of a target substrate within 10% accuracy in *Drosophila* embryos, given the morphogenic constraints that must be met (Gregor et al. 2007b). While steps have been made in characterizing existing GRNs (Gregor et al. 2007a; Zadorin et al. 2017; Chai et al. 2014), and even modifying existing cellular hardware to perform different types of circuit logic in vivo (Andrews et al. 2018), because of the breadth of dynamic functions that GRNs are capable of producing, research dedicated to the synthesis of new GRNs is also being conducted (Menolascina et al. 2011).

If the goal is to extract GRN functionality for use in other materials, or to simply expedite characterization of a GRN, one may consider in vitro GRNs, as performing cell-free expression allows for fast and quantitative experimentation (Garenne and Noireaux 2019). If the interest is in the design of dynamic materials, a synthetic chemical



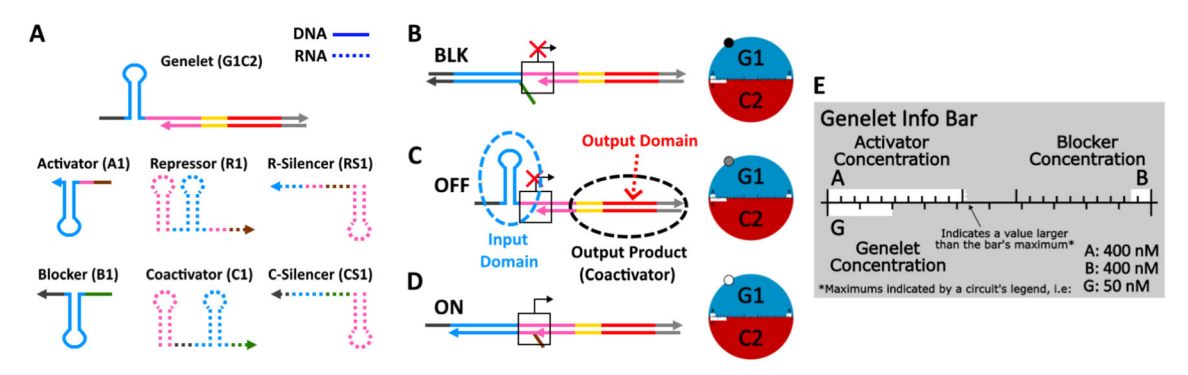


Fig. 1 Genelet circuit elements. A DNA (solid lines) and RNA (dashed lines) strands in an HPC5 genelet circuit, and their corresponding abbreviations. The input domain of a genelet determines which type of activator or blocker regulates its transcription rate. The output product sequence determines whether the resulting RNA is a repressor, repressor silencer (R-silencer), coactivator, and coactivator silencer (C-silencer) and which activator/blocker (domain) these products interact with. The input and the output domain of a genelet can be of different OCEs. B–D A genelet in the B BLK, C OFF,

D and ON states and their corresponding node representations in circuit diagrams. Boxes enclose the promoter regions of the genelet to indicate the conformation of the promoter region in each state, which determines its transcription activity. **E** The genelet info bar is a conventions used to describe the genelet concentration, as well as their associated activator and blocker concentration in a circuit diagram. A diagram key provides the maximum concentrations denoted by the respective bar

circuit mimicking the function of a in vitro GRN based on DNA may also be the desired approach, taking advantage of DNA's powerful selective binding through Watson-Crick base-pairing and DNA's well-studied interactions with other molecules (Jones et al. 2015; Seeman 2003). Several designs for DNA-based synthetic chemical circuits have been developed, including enzyme-free nucleic acid systems (Srinivas 2017; Cherry and Qian 2018), and in vitro transcriptional regulatory networks (TRNs) (Schaffter and Schulman 2019; Baccouche et al. 2014; Montagne et al. 2016).

One type of in vitro TRN which has been explored frequently is genelet circuits, a circuit scheme which takes advantage of existing enzymes such as T7 RNA Polymerase (RNAP) and RNase H to mediate the interplay of DNA and RNA molecules (Schaffter and Schulman 2019; Kim et al. 2006; Kim and Winfree 2011; Franco et al. 2011; Schaffter et al. 2022). A genelet refers to the subset of DNA molecules which act as templates for RNAP to transcribe, producing RNA products. Transcription is fueled by nucleoside triphosphates present in solution. The transcription templates are designed so that RNA products will perform complementary binding or toehold-mediated strand displacement (TMSD) with other DNA and RNA, regulating downstream genelet activity. These genelet circuits have been shown to work in vitro, demonstrated by the implementation of common circuit motifs such as bistable switches (Schaffter and Schulman 2019; Kim et al. 2006), oscillators (Kim and Winfree 2011; Franco et al. 2011), and incoherent feed-forward loops (Schaffter et al. 2022).

The standardization of genelet circuit elements in the form of HPC5 genelets (shown in Fig. 1A) have allowed

for the characterization and implementation of increasingly complex genelet circuits (Schaffter et al. 2022), where each element has been tested in vitro to meet certain kinetic behavior benchmarks. This standardization allows for increased genelet circuit scalability and designed modules to be interchangeable while following similar kinetics. Although possible design complexity has increased, such designs have not been extensively studied. Manifesting complex circuit behaviors would allow for material designs capable of orchestrating complex biosensing, morphogenesis, and multiplexing (Andrews et al. 2018; Khalil and Collins 2010). Each RNA product binds specifically to one type of upstream binding domain. We define sequences that direct this particular binding as orthogonal circuit elements (OCEs). Each genelet consists of an upstream binding domain and a product that regulates another genelet. A genelet is named by its upstream OCE (e.g. G1) followed by a product domain which consists of the regulation type and the OCE (e.g. C2), as seen in Fig. 1.

HPC5 genelets (Schaffter et al. 2022) have an activator that can bind to a genelet to complete a genelet's promoter sequence. This activator-genelet complex promotes the binding of RNAP, allowing for the RNA output of the particular genelet to be transcribed. Blocker inhibits the binding of activator by binding more favorably to the template due to the presence of a larger toehold on the blocker than the activator. Competitive binding by a blocker in turn downregulates the transcription of the given RNA output. Synthesized RNA can act directly or indirectly on downstream genelets (Schaffter et al. 2022). One type of such output RNA is a coactivator, which sequesters blocker to allow free activator strands to bind to a genelet (Fig. 2). Repressor can also be transcribed. Repressor



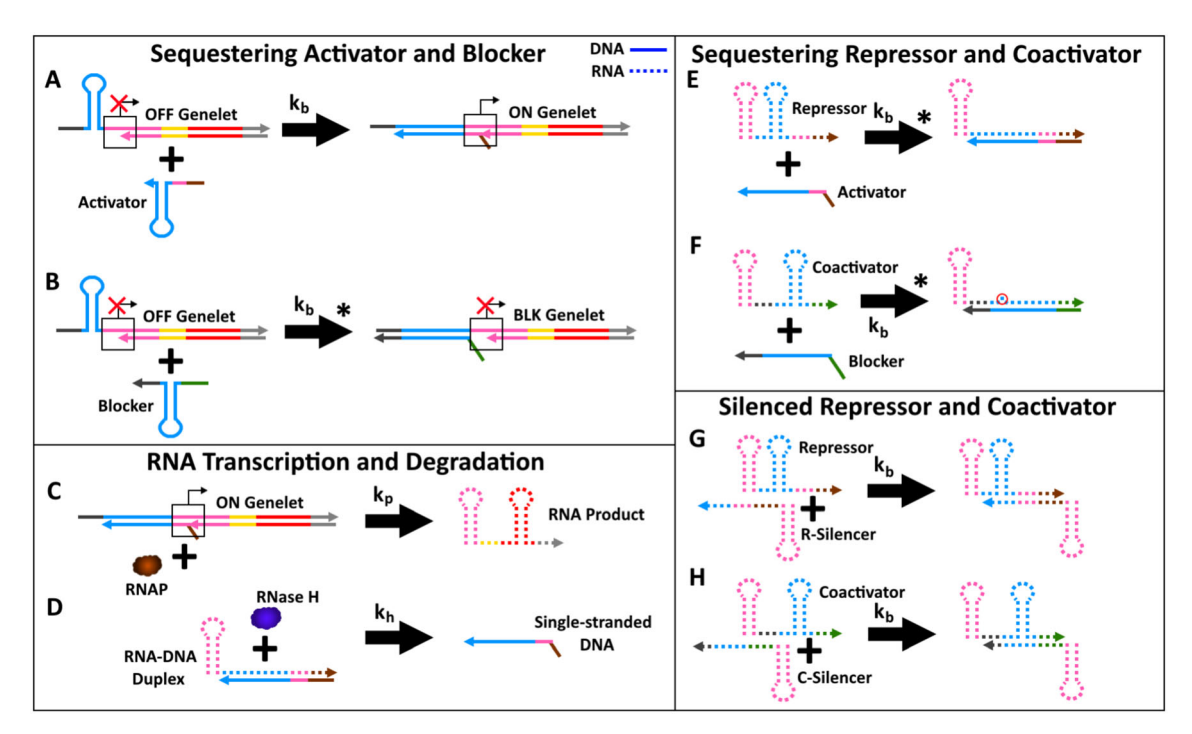


Fig. 2 Schematics of the relevant reactions simulated by the GGM (Schaffter et al. 2022). See Table 1 for the rates of reaction used in the GGM. A An activator binds to a genelet, thereby changing the genelet's state from OFF to ON. The blue region is the input domain of a given genelet, which corresponds with its activator and blocker, while the red region is the genelet's output domain. **B** A blocker binds to a genelet, thereby changing the genelet's state from OFF to BLK. Blocker binds more favorably than activator because the dark gray toehold domain has eight nucleotides, which is three more than the five exposed in the pink region for the activator, allowing the blocker to have favorable binding with the genelet. Reactions with a "*" (as shown here) indicate that the reaction can also proceed by the initial binding of the reactant toeholds (here the dark gray domain) followed by the displacement of an incumbent strand (here, the activator). In these cases, a rate constant of k_d is assumed. C An ON genelet is transcribed by T7 RNA Polymerase (RNAP). This will produce an RNA output product. In the case of this reaction, the product is an RNA coactivator. Not shown is the transcription of RNA repressor, C-silencer, and R-silencer. The pink region is an incomplete promoter for RNAP followed by an initiation sequence. The promoter region

sequesters activator, preventing activator from binding to its corresponding genelets even when no blocker is present. Each of these RNA strands can be sequestered from solution themselves by silencers, which can be transcribed or added to solution to sequester the complementary coactivator or repressor (Fig. 2) (Schaffter et al. 2022).

To predict the dynamic behavior of genelet circuits, the General Genelet Model (GGM) was created (Schaffter et al. 2022). The GGM is a mass-action kinetics model that models the reactions in Fig. 2 to predict the concentrations of each DNA/RNA species and complex over time. This model assumes that the solution is well-mixed and treats each OCE as having identical kinetics. The model has shown both qualitative and quantitative predictive power

must be completed by activator for the RNAP to favorably bind. In the model, we assume no transcription if this condition is not met. D RNA present in RNA-DNA duplexes, such as the RNA coactivator shown, will be continuously removed via catalyzed degradation by RNase H. E An RNA repressor binds to a DNA activator, preventing the activation of any associated genelets. This reaction is more favorable than activator-genelet binding because of the brown toehold present, which also allows for TMSD of the activator from ON genelets. F An RNA coactivator binds to a DNA blocker, preventing the blocker from inhibiting associated genelets. This is facilitated by the green toehold, allowing for TMSD of the blocker from BLK genelets. There is an intentional extra base pair in the coactivator, causing a disruptive misalignment. This was done to modify the binding kinetics, which is explained in Schaffter et al. (2022). G Rsilencer binds to a repressor, preventing the repressor from binding to its corresponding activator. H If C-silencer bound to a coactivator genelet, it would theoretically prevent the coactivator from binding to its corresponding blocker. While the reaction is included in the GGM, it was not experimentally demonstrated (Schaffter et al. 2022). (Color figure online)

for the genelet circuits tested in vitro. For example, genelet circuits that create tunable signal pulses using an IFFL motif have previously been demonstrated to function in vitro, the dynamics of which were successfully reproduced by the GGM (Schaffter et al. 2022). Thus, by using the model to predict dynamic circuit function, it is possible to explore the design space for other candidate circuits.

The GGM provides a route to systematically studying and designing mesoscale GRN analogs due to its demonstrated predictive power. Here we asked how one might design a specific genelet circuit with a complex function, using the GGM to evaluate designs. IFFL genelet circuits can generate a variety of pulses. A complementary circuit would be a detector that could discriminate between



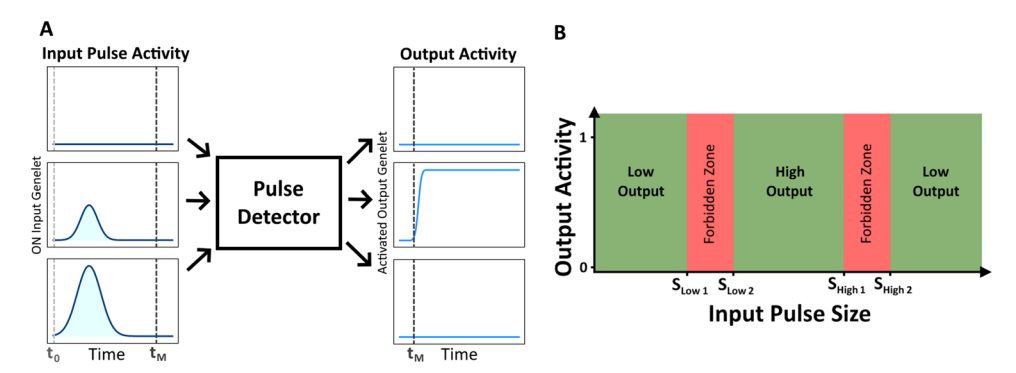


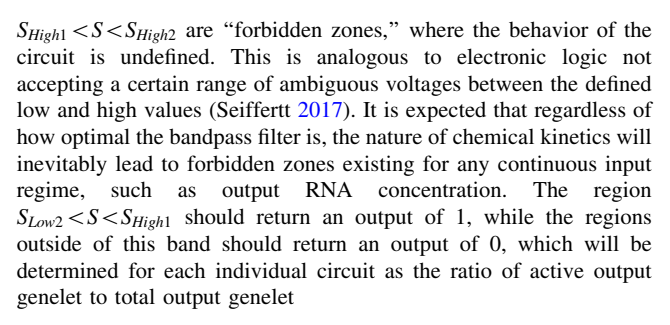
Fig. 3 Intended behavior of a genelet-based bandpass pulse detector. **A** Input pulse activity monitored by a set of genelets indicated by the black box labeled "Pulse Detector," which yields the resulting output profile. IFFL input pulse sizes are calculated by determining the area of the shaded region, i.e. integrating a pulse's activity over time. Low and high input pulse sizes are filtered from activating an output response, while medium signals will trigger output activity. Only input pulses of the intended size from the system's initialization t_0 to a time t_M lead to an output response after t_M . **B** We define input pulse size as an input genelet's total activity, which in the model is defined as the total output RNA created by the given genelet species (see Eq. 1). Input pulse sizes between $S_{Low1} < S < S_{Low2}$ and

different regimes of IFFL input pulse strength, by producing a sustained high output only for IFFL input pulses of a certain strength (Fig. 3). These types of circuits could allow for many interesting capabilities. For example, one could produce discrete state changes in a material based on a given signal substrate's absolute concentration, similar to how the precise absolute measurement of a substrate's concentration leads to specific sets of genes being expressed resulting in cell differentiation within Drosophila embryos (Gregor et al. 2007b). We approached this question by designing a concentration-based bandpass filter that responds to genelet IFFL pulses of particular sizes, referring to the area under the curve of a particular pulse. We used the GGM to demonstrate that a pulse detector design is feasible while working within reasonable design constraints. This pulse detector can be tuned to only recognize specific genelet IFFL pulse sizes by modifying just two of the DNA molecule concentrations in solution at the start of

2 Results

the simulated reaction.

When designing the circuit topology, the goal was to create a circuit where parameter tuning would lend itself to generating multiple variants of output profiles akin to the one displayed in Fig. 3. The parameter tuning regimes we limited ourselves to were genelet concentrations which were demonstrated experimentally before (Schaffter et al. 2022), giving us a range of 1–5000 nM for activator and blocker concentrations, and a range of 1–100 nM for



genelet concentrations. We also wanted to contain the circuit to a reasonable number of OCEs. In the context of these circuits, an OCE describes a specific genelet sequence and its family of strands that associate with its input domain. These include the activator and blocker associated with the genelet profile, as well as the corresponding RNA elements in solution which can interact with said activator and blocker or their respective silencers, see Fig. 1A. The reasoning for this imposed limitation is since there is a limited number of input domains whose functional properties were verified experimentally, and only select subsets of those which have been demonstrated to work simultaneously in in vitro circuits (Schaffter et al. 2022), the most attainable circuit would be one which could reuse OCEs from other successful large circuits.

While a bandpass filter's colloquial focus is on electronic circuits, specifically those that deal with a signal's frequency, here we are using the concept of a bandpass filter as a circuit which responds to a band of valid concentrations, as has been done previously (Shui et al. 2023; Greber and Fussenegger 2010). To construct a bandpass filter that differentiates between input pulse sizes, we defined a genelet's total activity as the total RNA produced by a dynamic concentration of ON genelet over the given simulation time. From here, we defined an input pulse's size as the total activity of any genelet whose input domain is designated to be activated and deactivated. This pulse's size can be determined by integrating over the RNA production rate from the initialization of the input (t_0) to its termination (t_M) . The GGM assumes that the rate of RNA production is proportional to the concentration of active



template for transcription. We defined the RNA production rate as a constant k_p multiplied by the concentration of ON genelet ($[G_{ON}]$) that produces the particular RNA in question, as shown in Eq. 1. We used the production rate listed in Table 1 from the GGM (Schaffter et al. 2022), which assumes a transcription rate of one RNA per genelet per 50 seconds to estimate calculate the pulse size, in total RNA concentration, that would be produced by a transcriptional circuit that turned on and then off in a pulsatile fashion (see SI Figure S1). We ignored the effects of RNase H degradation over time in this approximation

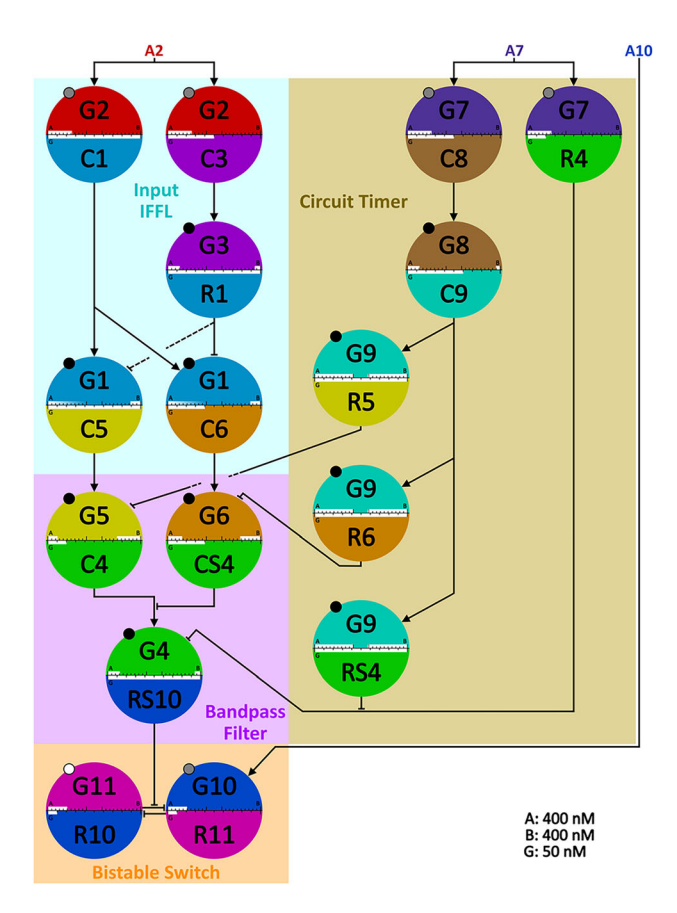


Fig. 4 Final pulse detector circuit topology with the input pulse generator. This collected circuit has four distinct modules: the input IFFL, the bandpass filter, the circuit timer, and the bistable switch. The input IFFL generates the pulses of varying size for the circuit to measure. The bandpass filter creates a transient response to the input IFFL, which is mediated by the circuit timer. The bistable switch then records whether a pulse within a given band was detected based on the final resulting node activity after time has passed. A2, A7, and A10 represent the unbound DNA activators added at the start of the simulation. This particular diagram represents a circuit that responds to an input pulse size band described as "medium" for the chosen range of input pulse sizes. SI Figures S2 and S3 provide variants of this circuit diagram which respond to low and high bands of input. The legend indicates the maximum concentrations that can be represented by the three respective bars in each genelet, as explained in Fig. 1

because we assumed that most RNA would not be bound to a DNA element and therefore would not be degraded.

[Output RNA] =
$$k_p \int_{t_0}^{t_M} [G_{ON}] dt$$
 (1)

The mechanism which differentiates between an input pulse size within the critical concentration and one outside of this concentration is the bandpass filter in Fig. 4.

We studied the case where a genelet IFFL produces the input pulse. We initially built a circuit that responds to input pulses. If an input pulse is of a sufficient size (greater than S_{Low2}), a low-threshold genelet is activated. However, if an input pulse is too large (greater than S_{High1}), a highthreshold genelet activates, which represses the output. The concentrations S_{Low2} and S_{High1} are controlled by the concentrations of the blockers for the low-threshold genelet and high-threshold genelet, respectively. Unfortunately, this design did not achieve the behavior specified in Fig. 3. This circuit did not achieve a sustained ON output for input pulses of sizes between S_{Low2} and S_{High1} . RNA output would be produced by the output genelet even when the input pulse size was greater than S_{High2} . To address these issues, we made a series of refinements to the original design. We added a bistable switch module layer to the circuit so that we would have a binary output as seen in prior literature (Kim et al. 2006; Schaffter et al. 2022), which would define if the pulse size was within the circuit's intended band of acceptable sizes. In addition, we addressed what we considered to be a failure in regulating a window in time for input by adding the "circuit timer" module, which would also maintain inactivity of the genelet leading up to the bistable switch until the requisite time had passed. Similar designs, using both kinetically delayed downstream signal transduction and the creation of a concentration barrier through threshholding, have been carried out both experimentally and computationally (Aubert et al. 2014; Fern et al. 2017; Scalise et al. 2020; Bucci et al. 2022). To allow for the circuit timer to function in this capacity, we modified the high-threshold genelet to produce coactivator silencer (C-silencer) instead of repressor, so that the timer could control the downstream genelet via the production of repressor and repressor silencer (R-silencer). The resulting final circuit topology is seen in Fig. 4.

The input is a pulse in the level of G1 ON activity. In our circuit, when G1 is on, both C5 and C6 are produced. The way the bandpass filter performs the pulse size measurement is through the use of a comparator-like switch. When input pulse genelets G1C5 and G1C6 are activated, they produce their respective coactivators at different rates. Since the concentration of G1C5 is greater than the concentration of G1C6, there will be more C5 produced than



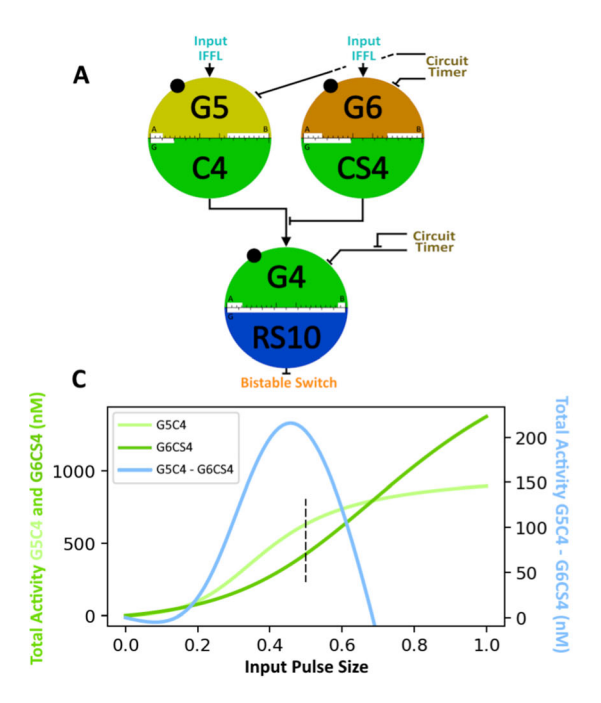
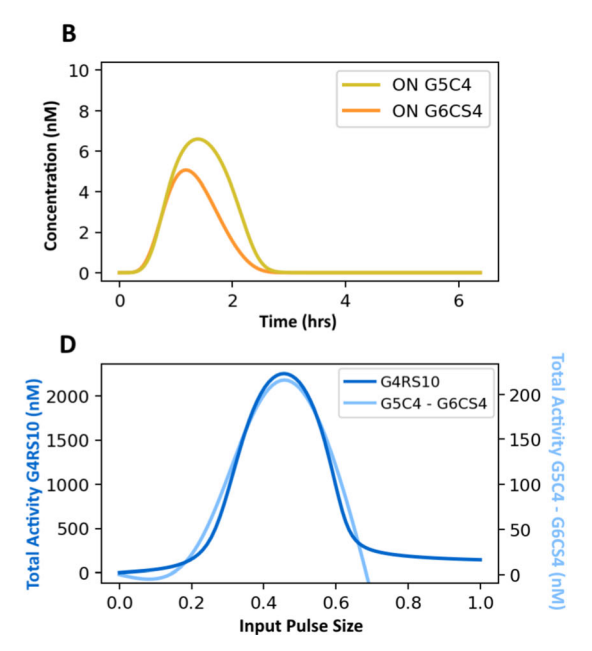


Fig. 5 Dynamics of the bandpass filter module over 101 simulations modulating input pulse size. We used the medium band design (Fig. 4) to generate these plots. **A** The bandpass filter of the circuit topology described in Fig. 4. C4 produced from ON G5C4 is sequestered from solution by CS4 produced from ON G6CS4. In order for downstream activity to occur, free C4 capable of removing downstream blocker from the G4RS10 node must be present.

C6. Conversely, the total concentration of G5C4 is less than that of G6CS4. This creates a dynamic where once input pulse sizes are large enough that G5C4 is producing significant amounts of C4, it will initially have a production advantage over G6CS4. However, G5C4's maximum production is capped at a lower rate than G6CS4 due to the respective genelet concentrations, so if the pulse size is sufficiently large that G6CS4's blocker is fully sequestered, G6CS4 will have the net production advantage, as seen in Fig. 5C. Thus, only when the pulse size is sufficiently large, but does not exceed the designated threshold size, free C4 is present in solution (for additional context, see SI Figure S4).

However, this comparison only works when both G5C4 and G6CS4 are given sufficient time to have their products interact after the entire pulse has been received (i.e. t_M in Fig. 3). While the pulse is being produced, C4 will be in excess, which could trigger a positive output of the pulse detector before the entire pulse completes. Furthermore, after t_M , the bandpass filter will still be comparing through the production of C4 and CS4, which could lead to spurious activity of G4RS10 long after the intended measurement time t_M . The circuit timer resolves these issues by adding an additional layer of control over this measurement process.



B Activity over time for G5C4 and G6CS4 with respect to an input pulse size of 0.5 (725 nM total C5 produced from G1C5). **C** Total activity of G5C4 and G6CS4 as well as their difference, calculated using Eq. 1 across the input pulse sizes of interest. **D** The difference in G5C4 and G6CS4 activity compared with the total activity of G4RS10 across the input pulse sizes of interest

The circuit timer's input genelets, G7C8 and G7R4, are triggered at the same time as the input pulse. G7R4 is present in low concentration to passively generate R4 at a rate that keeps G4RS10 from activating early, but is susceptible to quick suppression by RS4, which is produced at much higher rates when activated. The concentration of B9 is sufficient to prevent significant activation of the downstream G9 genelets until a requisite amount of time has passed. The concentration of free B9 decreases as the upstream coactivator, C9, is produced (see SI Figure S1E). Once a critical concentration of C9 has been produced, genelets G9R5 and G9R6 activate. These genelets respectively repress G5C4 and G6CS4 in the bandpass filter module.

The timer module also prevents G4RS10 (i.e. the bandpass filter module's output) from turning ON until t_M is reached. G8C9 also activates G9RS4, which inhibits the repression of the downstream genelet G4RS10 until t_M . Therefore, the relative activities of G5C4 and G6CS4 between t_0 and t_M determine how much C4 and CS4 are produced, which in turn determines the amount of B4 that is sequestered (by binding to C4). If enough B4 is sequestered, G4RS10 is activated. The total activity of G4RS10 only exceeds a specific threshold when the input pulse size is between S_{Low2} and S_{High1} .



If G11R10, which is initially biased to be active over G10R11, has its R10 products sequestered by RS10, this will lead to the activity profile of the bistable switch being inverted. What qualifies as sufficient is dictated by the amount necessary to lead to enough downstream activity in G4RS10, which will toggle the bistable switch, so that G10R11 turns ON and stays ON indefinitely. When G10 is ON, the output of the pulse detector is ON.

To demonstrate the functionality of this new circuit, we chose to create pulse sizes only through the modification of A1 concentration and measure the response to a given set of concentrations. This means that all pulses were generated using the same IFFL motif as presented in Fig. 4, but approximations for pulse size were made using Eq. 1 to measure G1C5 activity. We simulated 61 linearly distributed initial free A1 concentrations from 0 to 330 nM, yielding total output RNA production from ON G1C5 in a range of 0 nM to 1252 nM. All input pulse sizes presented are given on a scale from 0 to 1, which is the result of a given RNA output being normalized by the maximum RNA output of G1C5 (1252 nM). The total RNA output of G1C5 is different from the total RNA output of G1C6 since the genelets are present at different concentrations, but they are directly proportional to each other due to having the same input domain, so the RNA output of G1C5 was chosen as the sole input metric for simplicity. To monitor the behavior of the bandpass filter, we chose to compare the resulting activity of the G5C4 node and G6CS4 nodes with the given pulse size for a given bandpass design, as seen in Fig. 5.

The concentrations of B5 and B6 control the lower and upper bounds respectively of the pulse size band being detected. We measured the activity of G10R11 at 10 h from the circuit's start time (t_0 as depicted in Fig. 3A) with a range of input pulse sizes for three pulse detector variants with three different bands of concentrations (different S_{Low2} and S_{High1} as depicted in Fig. 3B). The resulting fraction ON G10R11 at 10 h is shown in Fig. 6A. For each variant, the circuit produced a high output when input pulse size was between S_{Low2} and S_{High1} . As designed, the total activity of G4RS10, which we refer to as the bandpass activity, exceeds a threshold value only when the input pulse is between S_{Low2} and S_{High1} for that variant (Fig. 6B). The simulated bandpass filters have behaviors that qualitatively matched the ideal case described in Fig. 3. The underlying activity determining the final state of the bistable switch is that of G4RS10, whose activity is determined by upstream nodes G5C4 and G6CS4,

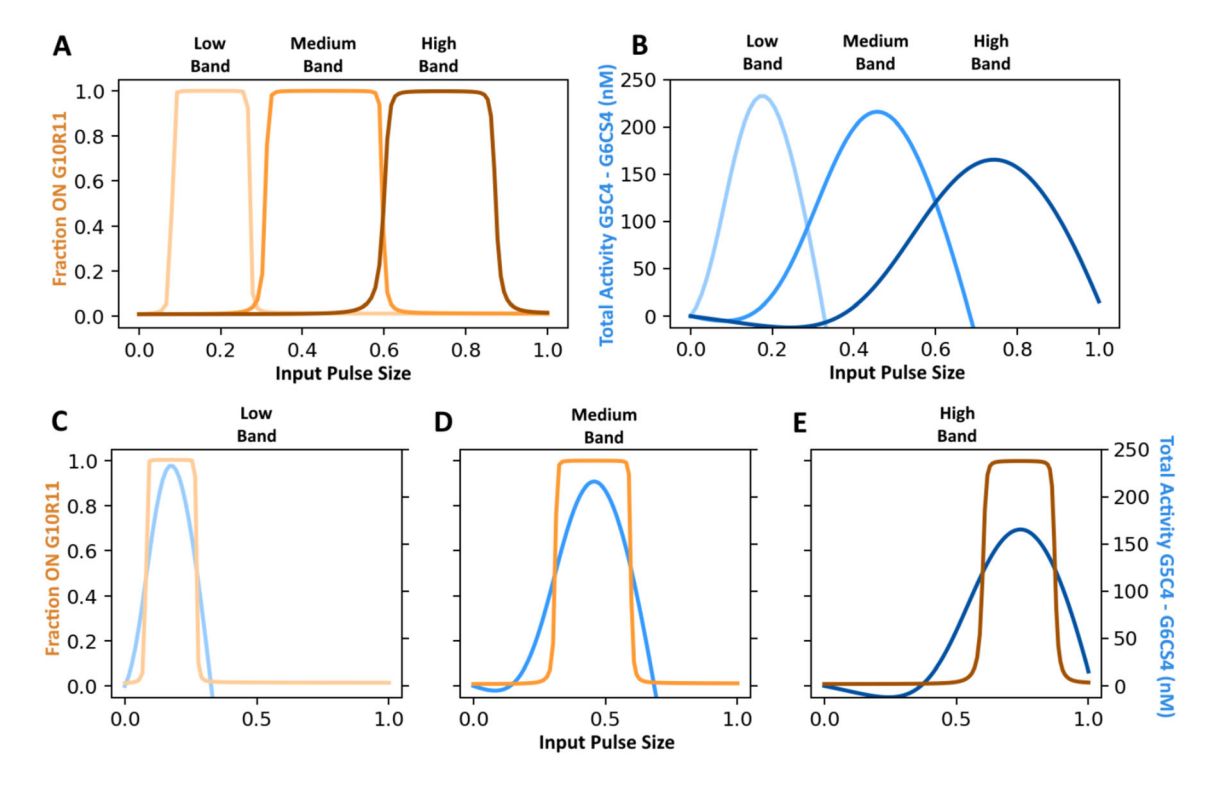


Fig. 6 A G10R11 bound to activator (Fraction ON) at 10 h in the simulation vs. input pulse size. Low, medium, and high band circuits correspond to the blocker concentrations B5 and B6 found in Table 3. All other concentrations for each circuit can be found in Table 2. **B** Total difference in activity of G5C4 and G6CS4 for all three

circuits vs. input pulse size. Comparison of C low, D medium, E and high band fraction ON G10R11 at 10 h from Fig. 6A with total activity differences from Fig. 6B. Peaks in comparator activity align with the middle of the target input bands



demonstrated in Fig. 5D. We also compared the fraction of ON G10R11 at 10 h with the bandpass activity, as seen in Fig. 6C.

Thus, we built a bandpass filter capable of discriminating between ranges of input pulse sizes, and the range of input pulse sizes to which the circuit will respond are chosen by selecting the appropriate concentrations of B5 and B6. We were able to tune this threshold by tuning the bandpass activity (Fig. 6B). The bandpass activity was tuned indirectly by modifying the concentrations of the B5 and B6, thus obtaining the designated bands in Fig. 6C–E.

3 Discussion

When constructing an in vitro GRN with predictable behavior, one of the main concerns in implementing the described circuit function experimentally is the elimination of unwanted side reactions by having a set of OCEs that have very limited binding compatibility with one another (Schaffter et al. 2022). This restriction decreases the odds of unintended behaviors such as crosstalk between genelets to occur, leading to unintended circuit dynamics not predicted by the model. It is vital that the number of OCEs be kept to a minimum in GRN design such that there is less of a chance for unintended non-orthogonal behavior when designs are tested in vitro, and it can eliminate the need to identify additional OCEs if the given GRN extends beyond the known number of OCEs used in prior literature (Schaffter et al. 2022).

Consequently, it is important that each OCE added to a circuit needs to have a crucial purpose, and that a given circuit's defined function space may not be replicated using fewer OCEs. While the topology space for the pulse detector's design was thoroughly probed and we believe each genelet included performs a necessary function, it is by no means a guarantee that this topology uses the fewest OCEs necessary to elicit the full complement of desired behaviors. Further analysis will need to be conducted to examine the network topology space and establish an absolute minimum number of OCEs.

Currently, while the GGM predicts the results of a C-silencer being present in solution, this particular silencer's in vitro design has not yet been engineered. For the scope of this paper we assumed that a C-silencer would have analogous design and behavior to an R-silencer (formerly referred to as an "inducer" Schaffter et al. 2022), including a matching binding constant for a C-silencer's sequestration of coactivator (see Fig. 2). This structure's

viability will have to be reexamined when making modifications as a result of the designed in vitro C-silencer.

Another design challenge that will need to be addressed for this circuit to be integrated with others is the replacement of the G7C8 OFF genelet with a circuit element that syncs the input with the activation of the timer. For the purposes of the simulation, it was assumed that activator for the G2 nodes and G7 nodes are added simultaneously. It is possible that G7C8 activity could be controlled indirectly with the presence of a bistable switch (G7R_ and G_R7, where _ is an additional domain), which would flip in activity in the presence of an input signal.

Tuning the various circuit concentrations (activator, blocker, and genelet totals) to get the desired behavior for a particular bandpass filter iteration can be tedious. The approach that yielded three circuits whose defining concentrations can be found in Tables 2 and 3 was a combination of intuition and trial-and-error, with the circuit's design guiding the sets of parameters we used. We wanted to make sure that the regime chosen was based on the regimes that had been previously tested, and that they were flexible in the case of expected deviations in component concentrations. Once we settled on a reasonable concentration regime for the majority of the circuit components, we modified the concentrations of B5 and B6 to create the low, medium, and high bandpass domains. This was on the basis of these blocker concentrations serving as the thresholds for the respective low and high bounds of each bandpass circuit. The relationship between the pulse size bound being targeted and the concentration of the given blockers is not linear, so some testing was required to find the displayed bands.

Further work will need to be completed to allow for a given bandpass filter to be generated on demand via an optimization algorithm that tunes for the desired pulse size. It is also likely that other circuit element concentrations are tunable to modify the bandpass's low and high bounds, but could result in non-intuitive changes to other circuit behaviors as well. We plan on experimentally testing the individual circuit components and establishing a repository of individual kinetics for the genelet strands we choose. Using the topologies developed here, we can guide our approach to creating an in vitro bandpass filter.

Appendix

See Tables 1, 2 and 3.



Table 1 List of reaction rates

Constant	Value
k_b	10,000 (M Duplex _{new}) * (M ssN ₁) ⁻¹ * (M ssN ₂) ⁻¹ * s ⁻¹
k_p	0.02 (M RNA) * $(M G_{ON})^{-1} * s^{-1}$
k_h	0.0003 (M ssDNA) * $(M RNA-DNA Duplex)^{-1} * s^{-1}$
k_d	5000 (M Duplex _{new}) * (M ssN ₁) ⁻¹ * (M Duplex) ⁻¹ * s ⁻¹

[&]quot;ss" refers to single-stranded, N_1 and N_2 refer to the nucleic strands of interest performing the binding. Kinetics assumed are identical to the default kinetics listed in Schaffter et al. (2022)

Table 2 List of concentrations used in all three analyzed topologies (low, medium, and high band circuits)

Genelet	Conc. (nM)		
G2C1			
	50		
G2C3	25		
G3R1	23		
	50		
G1C5	50		
G1C6	30		
0100	20		
G5C4	10		
G6CS4	10		
00034	20		
G7R4			
67.00	10		
G7C8	25		
G8C9			
G07.5	30		
G9R5	50		
G9R6			
	50		
G9RS4	50		
G4RS10			
	10		
G10R11	5		
G11R10	3		
	5		
Activator	Conc. (nM)	Blocker	Conc. (nM)
A1	I.V.	B1	105
A2	250	B2	0
A3	125	В3	75
A4	50	B4	35
A5	100	B5	I.V.



Table 2 (continued)

Activator	Conc. (nM)	Blocker	Conc. (nM)
A6	150	В6	I.V.
A7	250	В7	0
A8	125	В8	45
A9	400	В9	1925
A10	200	B10	0
A11	200	B11	0

Concentrations listed as "I.V." (independent variable) were modified to change the input or the circuit's target band. The concentration of A1 was changed to vary the input pulse size for each of the bandpass filters to capture circuit performance. B5 and B6 concentrations are changed to differentiate the targeted pulse size band of the given circuit topology (see Table 3)

Table 3 List of concentrations (in nM) for circuit elements B5 and B6 used in the low, medium, and high band circuit designs

Component	Low band	Medium band	High band
B5	85	205	335
B6	130	200	280

These two parameters dictate the amount of C5 and C6 needed for activation of G5C4 and G6CS4, and thus roughly control the lower and upper bounds of each band. By increasing the blocker for one of these OCEs, the respective bound is increased

Supplementary Information The online version contains supplementary material available at https://doi.org/10.1007/s11047-024-09992-3.

Acknowledgements The authors thank Sam Schaffter, Yan Xiong, Heon Joon Lee, Kuan-Lin Chen, Emily Helm, and Mingzhi Zhang for their helpful comments on the manuscript.

Author contributions Colin Yancey and Rebecca Schulman designed the research and prepared the manuscript. All simulations, their results, and their figures were made and/or formatted by Colin Yancey. Both authors reviewed the manuscript.

Funding The authors are grateful for the financial support of the National Science Foundation (NSF) award CIF-2107246, the NSF Graduate Research Fellowship Program award DGE-2139757, and the Army Research Office award W911NF-22-2-0111. Any opinions, findings, and conclusions or recommendations expressed in this material are those of the authors and do not necessarily reflect the views of the United States Army or the National Science Foundation.

Data availibility All code used to create the plots in Figs. 5 and 6, and SI Figures S1 and S4, is available on GitHub at https://github.com/YanceyColin/PulseDetector.

Declarations

Conflict of interest The authors declare no Conflict of interest.

Ethical approval Not applicable.

Open Access This article is licensed under a Creative Commons Attribution 4.0 International License, which permits use, sharing, adaptation, distribution and reproduction in any medium or format, as long as you give appropriate credit to the original author(s) and the

source, provide a link to the Creative Commons licence, and indicate if changes were made. The images or other third party material in this article are included in the article's Creative Commons licence, unless indicated otherwise in a credit line to the material. If material is not included in the article's Creative Commons licence and your intended use is not permitted by statutory regulation or exceeds the permitted use, you will need to obtain permission directly from the copyright holder. To view a copy of this licence, visit http://creativecommons.org/licenses/by/4.0/.

References

Andrews L et al (2018) Cellular checkpoint control using programmable sequential logic. Science 361(6408):eaap8987

Aubert N et al (2014) Enforcing logical delays in DNA computing systems. Nat Comput 13:559–572

Baccouche A et al (2014) Dynamic DNA-toolbox reaction circuits: a walkthrough. Methods 67(2):234–249

Bucci J et al (2022) Orthogonal enzyme-driven timers for DNA strand displacement reactions. J Am Chem Soc 144(43):19791–19798

Chai LE et al (2014) A review on the computational approaches for gene regulatory network construction. Comput Biol Med 48:55-65

Cherry K, Qian L (2018) Scaling up molecular pattern recognition with DNA-based winner-take-all neural networks. Nature 559(7714):370–376

Fern J et al (2017) DNA strand-displacement timer circuits. ACS Synth Biol 6(2):190–193

Franco E et al (2011) Timing molecular motion and production with a synthetic transcriptional clock. Proc Natl Acad Sci USA 108(40):E784–E793

Garenne D, Noireaux V (2019) Cell-free transcription–translation: engineering biology from the nanometer to the millimeter scale. Curr Opin Biotechnol 58:19–27

Greber D, Fussenegger M (2010) An engineered mammalian bandpass network. Nucleic Acids Res 38(18):e174

Gregor T et al (2007a) Stability and nuclear dynamics of the bicoid morphogen gradient. Cell 130(1):141–152

Gregor T et al (2007b) Probing the limits to positional information. Cell 130(1):153–164

Jones M et al (2015) Programmable materials and the nature of the DNA bond. Science 347(6224):167–197

Khalil A, Collins J (2010) Synthetic biology: applications come of age. Nat Rev Gen 11(5):367-379

Kim J, Winfree E (2011) Synthetic in vitro transcriptional oscillators. Mol Syst Biol 7:465



- Kim J et al (2006) Construction of an in vitro bistable circuit from synthetic transcriptional switches. Mol Syst Biol 2:68
- Menolascina F et al (2011) Analysis, design and implementation of a novel scheme for in-vivo control of synthetic gene regulatory networks. Automatica 47(6):1265–1270
- Montagne K et al (2016) Boosting functionality of synthetic DNA circuits with tailored deactivation. Nat Commun 7:13474
- Scalise D et al (2020) Programming the sequential release of DNA. ACS Synth Biol 9(4):749–755
- Schaffter S et al (2022) Standardized excitable elements for scalable engineering of far-from equilibrium chemical networks. Nat Chem 14(11):1224–1232
- Schaffter S, Schulman R (2019) Building in vitro transcriptional regulatory networks by successively integrating multiple functional circuit modules. Nat Chem 11(9):829–838
- Seeman N (2003) DNA in a material world. Nature 421(6921):427–431
- Seiffertt J (2017) The digital electronic computer. Springer, Berlin

- Shui S et al (2023) Protein-based bandpass filters for controlling cellular signaling with chemical inputs. Nat Chem Biol. https://doi.org/10.1038/s41589-023-01463-7
- Sladitschek H, Neveu P (2019) A gene regulatory network controls the balance between mesendoderm and ectoderm at pluripotency exit. Mol Syst Biol 15(12):e9043
- Srinivas N (2017) Enzyme-free nucleic acid dynamical systems. Science 358(6369):eaal2052
- Ueda Y et al (2020) Gene regulatory network and its constituent transcription factors that control nitrogen-deficiency responses in rice. New Phytol 227(5):1434–1452
- Zadorin A et al (2017) Synthesis and materialization of a reaction—diffusion French flag pattern. Nat Chem 9:990–996

Publisher's Note Springer Nature remains neutral with regard to jurisdictional claims in published maps and institutional affiliations.

